# Generating 275-m Resolution Land Surface Products From the Multi-Angle Imaging SpectroRadiometer Data

Michel M. Verstraete, *Senior Member, IEEE*, Linda A. Hunt, Robert J. Scholes, Marco Clerici, Bernard Pinty, and David L. Nelson

***Abstract*—This paper shows how to reconstruct the original 275-m resolution data of the Multi-angle Imaging SpectroRadiometer (MISR) instrument in the 24 spectrodirectional global mode channels that are spatially averaged to 1.1 km on-board the Terra platform, with negligible loss of information relative to images acquired in native-resolution local mode. Standard approaches to improve the spatial resolution of products rely on one (typically panchromatic) high-resolution (HR) image to sharpen multiple spectral images. In the case of the MISR-HR package described here, three of the 12 available HR channels are combined to regenerate each of the 24 reduced-resolution channel to its native resolution. The accurate and rigorously reconstructed spectral bidirectional reflectance data allow sensitive and physically meaningful land surface attributes to be recovered at a spatial resolution appropriate to document the spatial heterogeneity of the land surface and relevant for climate and environment studies. MISR has been in continuous operation since February 2000 and provides global coverage in at most nine days (depending on latitude). This technique allows the generation of quantitative information to monitor change and model ecosystem function virtually anywhere and at any time during the last decade. The potential is demonstrated for a savanna landscape in South Africa.**

***Index Terms*—Africa, Earth observing system, ecosystems, high-resolution imaging, inverse problems, spectroradiometers, vegetation mapping.**

## I. Introduction

THE interaction of the land surface with the atmosphere and the production of plant biomass through the process of photosynthesis are fundamentally influenced by the magnitude and seasonal variation of variables such as the albedo, the fraction absorbed photosynthetically active radiation (FAPAR), and the leaf area index (LAI). These land surface properties vary appreciably over distances of tens to hundreds of meters and on a range of time scales from days to months. They are ideally suited for monitoring through space-based remote sensing, and this is one of the main rationales for a class of moderate-resolution polar orbiting Earth observation satellites operating in the solar spectral range. The most widely used products, because of their ready availability, moderate spatial resolution, and long history of use, are various vegetation indices, which have an indirect and variable relationship with the actual parameters of interest. It is, however, possible, using the same spectral information, to estimate the key geophysical variables of interest directly. Doing so in a rigorous way requires correcting for (and using the information in) the differences in surface reflectance resulting from varying sun-surface-sensor geometries [embodied in the bidirectional reflectance factors (BRFs)]. Most researchers using nadir-pointing sensors do this by *assuming* the angular distribution of the BRF and then by correcting the views on successive orbits to a standard geometry. The Multi-angle Imaging SpectroRadiometer (MISR) instrument is unique among currently operating sensors in that it simultaneously captures spectral reflectances at nine different angles, allowing for an enhanced characterization of the surface anisotropy, and, therefore, a better constrained retrieval of land surface products, with a documented uncertainty, compared to traditional products. The drawback thus far was that the MISR standard products have a downgraded resolution of 1.1 km over land (and coarser for higher level products), which is often too coarse to capture land surface heterogeneity. This paper shows that land surface products can be retrieved at the native resolution of 275 m of that sensor, using the existing global long-term archive of MISR data, and therefore support environmental applications that can take advantage of this enhanced resolution.

Manuscript received June 13, 2011; revised September 9, 2011 and February 24, 2012; accepted February 26, 2012. Date of publication April 12, 2012; date of current version September 21, 2012.

M. M. Verstraete is with the Institute for Environment and Sustainability, Joint Research Centre, European Commission, 21027 Ispra (VA), Italy (e-mail: Michel.Verstraete@jrc.ec.europa.eu) and was on sabbatical leave at the Natural Resources and the Environment (NRE) of the Council for Scientific and Industrial Research (CSIR) in Pretoria 0001, South Africa, in 2011.

L. A. Hunt is with the Science Systems and Applications, Inc., Hampton VA 23666 USA.

R. J. Scholes is with the Council for Scientific and Industrial Research, Pretoria 0001, South Africa.

M. Clerici is with the Institute for Environment and Sustainability, Joint Research Centre, European Commission, 21027 Ispra (VA), Italy.

B. Pinty is with the Institute for Environment and Sustainability, Joint Research Centre, European Commission, 21027 Ispra (VA), Italy and was detached at ESA ESRIN, 00044 Frascati (Rm), Italy in 2011.

D. L. Nelson is with the NASA Jet Propulsion Laboratory, Pasadena, CA 91109 USA.

Digital Object Identifier 10.1109/TGRS.2012.2189575

## II. MISR Instrument and Standard Products

The MISR instrument, built by the Jet Propulsion Laboratory (JPL), is hosted on the NASA Terra platform, which was launched on December 18, 1999. The polar sun-synchronous orbit of this platform follows a 16-day repeat cycle and crosses

the Equator at 10:30 A.M. (local time). During this cycle, the platform follows 233 different paths, after which the pattern repeats itself. Data and products from orbits belonging to the same path refer to exactly the same geographical area, observed from the same angles, while data and products from successive orbits provide the spatial and temporal coverage. The platform orbits around the Earth 14.6 times per day, and MISR has been in essentially continuous operation since February 2000. All data products and extensive documentation are hosted at and freely available from the NASA Langley Atmospheric Science Data Center.

MISR acquires data from the sunlit side of the Earth. This instrument has been extensively described in the refereed literature (e.g., [1] and [2]), and the suite of standard products is documented in a complete set of Algorithm Theoretical Basis Documents (ATBDs) available from http://eospso.gsfc.nasa.gov/eos_homepage/for_scientists/atbd/. MISR features nine cameras pointing at various angles (Df: 70.3°, Cf: 60.2°, Bf: 45.7°, Af: 26.2°, An: 0.1°, Aa: 26.2°, Ba: 45.7°, Ca: 60.2°, and Da: 70.6°, forward and aft of the platform, each one equipped to acquire data in four spectral bands of 20–40 nm full width at half height: blue (446.4 nm), green (557.5 nm), red (671.7 nm), and near-infrared (866.4 nm) [3]). The common swath width between the nine cameras is about 385 km wide. The revisit frequency for a given site depends on its latitude and varies from about two days near the poles to nine days at the Equator.

The ground sampling distance (often incorrectly referred to as spatial resolution) of the sensor across-track is 275 m at all off-nadir angles and 250 m for the nadir camera. The ground sampling distance along-track is 275 m for all cameras, although the footprint of each camera pixel on the geoid ranges from 214 (An camera) to 707 m (D cameras) along-track. Raw data are deconvoluted and resampled to the Space Oblique Mercator (SOM) projection in the process of generating level 1B2 products, at which point all products are provided at the nominal spatial resolutions of 275 or 1100 m. We will refer to the 275-m resolution as the "native" MISR resolution.

In global mode (GM) operation, which is the default case, the data transmitted to the ground segment are partially averaged on-board as follows to reduce the overall instrument data rate: the nonred spectral bands of the off-nadir pointing cameras are spatially averaged over areas of $4 \times 4$ pixels to yield an effective spatial resolution of 1.1 km. However, all four spectral bands of the nadir pointing camera and the red channel of all off-nadir cameras are downloaded at the native resolution [3]. Furthermore, the MISR instrument can occasionally be run in the so-called local mode (LM) of operation, where all 36 channels are acquired at the native resolution of the sensors over a limited geographical area: LM scenes feature the same 385-km-wide swath width, extend for about 300 km along-track, and are typically acquired at most once per orbit.

Raw data (level 0) are processed into products of greater geophysical significance or wider appeal for practical applications: level 1B2 products are calibrated and georeferenced spectral and directional radiances at the nominal "top of the atmosphere" (TOA) and at whatever spatial resolution is available from the mode of operation (global or local). Level 2 products are geophysical variables documenting the state of the atmosphere or surface at the 1.1-km (or coarser) resolution, while level 3 products provide much more synthetic information in the form of statistics, aggregated in space and time, which are suitable for downstream applications such as global climate modeling. The procedures used to generate these products are fully documented in the ATBDs. LM products are available only at level 1B2. While MISR products are typically stored as full orbits, data files can be ordered for smaller regions called blocks, which are consecutive areas of about 385 km (across-track) by 140.8 km (along-track) along the full orbit. Some 180 blocks are defined for each orbit, although not all contain useful data at any given time because of the seasonal changes in illumination at the poles.

Exploiting the multiangular capability of MISR clearly requires that the measurements acquired by the various cameras be coregistered. Level 1 and 2 products are georectified to the SOM projection to minimize distortions and resampling effects while allowing data acquired in different spectral bands or at different angles to be effectively colocated. This can be achieved either by focusing all cameras on the reference ellipsoid or on the actual terrain surface, taking topography into account. Both versions of these products are systematically generated and available from the NASA LaRC ASDC.

At level 1, one-third of all observations (the four spectral channels of the nadir pointing camera and the red channel of the eight off-nadir cameras) are thus systematically acquired at the full spatial resolution of the sensor, while the remaining 24 data channels are transmitted as spatial averages. The goal of this paper is to show that all 36 TOA radiance of reflectance values can be provided at the native spatial resolution with a good accuracy and that this technique offers new opportunities to investigate environmental issues (anywhere on the planet and at any time during the last 12 years, provided the sensor has a noncloudy view of the surface) at a spatial resolution 16 times higher than the "standard" global products typically available at the 1.1-km resolution. The usefulness of this approach is showcased by investigating environmental issues in and around the Kruger National Park in South Africa.

## III. DATA

For the purpose of this paper, we have downloaded blocks 110 and 111 of all available orbits between March 8, 2000, and August 18, 2010, along paths 168 and 169 for L1B2 (TOA) and L2 (land surface) reflectance products, both in "Terrain" projection. These blocks cover a reasonably large area around Skukuza, a research field site (latitude: $25°01'10.80''$S, longitude: $31°29'48.60''$E) within the Kruger National Park maintained by South Africa's Council for Scientific and Industrial Research (CSIR) featuring a flux tower equipped with $CO_2$, radiation, wind, and other standard instruments. An AERONET station is also available nearby, and the biology and ecology of the site have been thoroughly documented over a number of years (e.g., [4]–[6]).

In addition, MISR LM data for the same area have been systematically acquired since December 30, 2009, for the purpose of examining the performance of the sharpening algorithm described in the following. All data were acquired

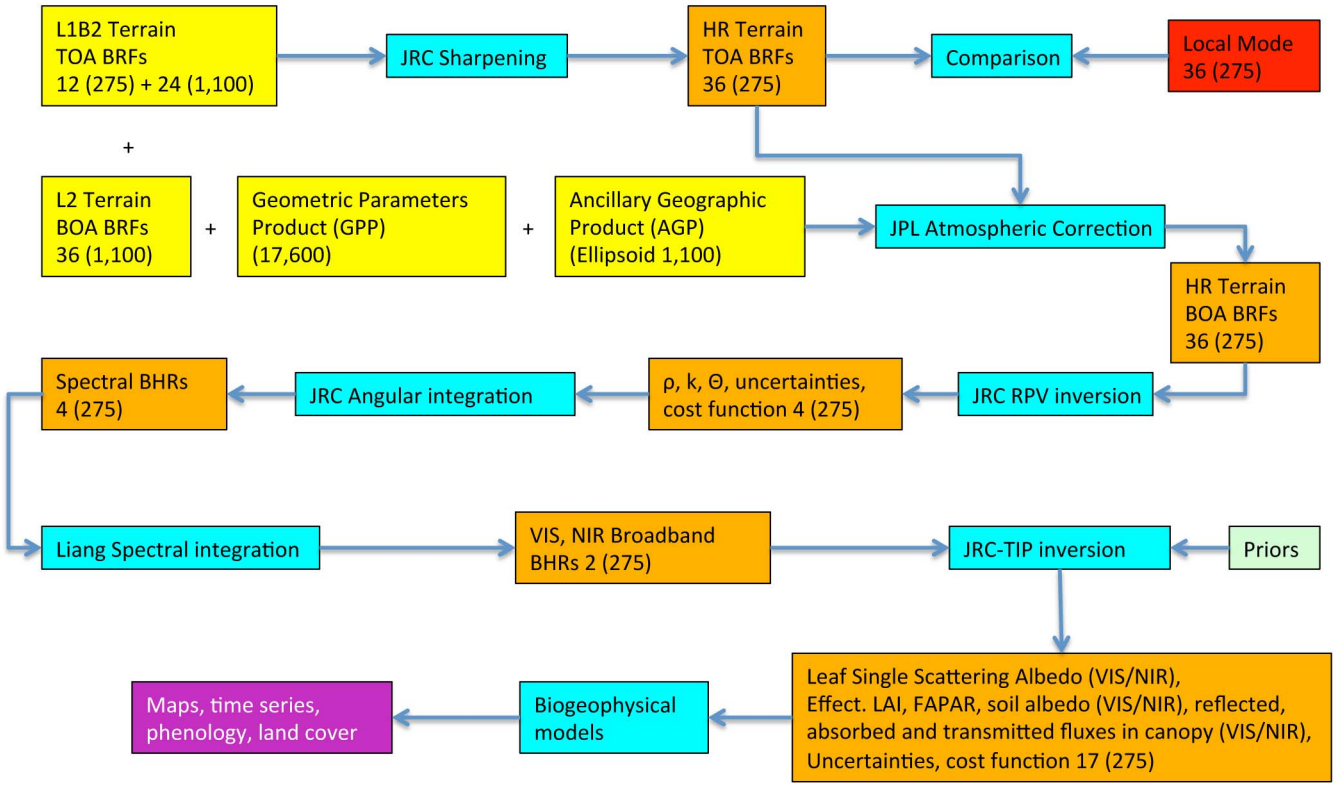


Fig. 1. Overview of the MISR-HR processing system. The yellow boxes represent inputs from standard MISR GM products; the red box refers to LM data, which are used only for evaluation purposes; the orange boxes represent the new high spatial resolution (275 m) products generated in this context; the cyan boxes indicate computational models or codes; the light green box stands for external prior estimates of JRC-TIP model values; and the final purple box includes all postprocessing steps associated with particular user-driven applications. The numbers at the bottom of each data box indicate the number of channels or values available for each pixel, at the spatial resolution indicated in parentheses. In this diagram, L1B2 and L2 refer to standard levels of data processing, JRC refers to the Joint Research Centre, HR is the acronym used in this document to refer to high-resolution products, BOA and TOA stand for bottom and top of atmosphere, respectively, BRF and BHR refer to the bidirectional reflectance factor and bihemispherical reflectance, respectively, VIS and NIR mean visible and near-infrared spectral bands, JRC-TIP points to the package described in the text and associated references, and LAI and FAPAR refer to leaf area index and fraction of absorbed photosynthetically active radiation, respectively. See text for details.

from the NASA Langley Atmospheric Science Data Center in Hampton, VA.

## IV. Processing

The flowchart in Fig. 1 shows an overview of the MISR-HR software environment that has been designed and implemented to process MISR GM data. The key steps include the following: 1) the 24 nonred and nonnadir data channels that were spatially averaged (to 1.1 km) on the platform before transmission to the ground are first sharpened to regenerate estimates of the original values at the full spatial resolution of the sensor (275 m); 2) all 36 high-resolution (HR) channels are then "atmospherically corrected," taking advantage of the existence of the standard L2 product which is already processed, albeit at the coarser spatial resolution; 3) the anisotropy of the surface is characterized at the full spatial resolution by inverting a BRF model against these data in each of the four spectral bands; 4) the corresponding spectral surface albedos are computed through directional integration, and the broadband albedos in two spectral bands (visible and near infrared) are estimated by spectral integration; and, finally, 5) the JRC-TIP approach is exploited to derive a set of internally consistent geophysical products characterizing the observed environment at the full spatial resolution.

### A. Sharpening the 1.1-km L1B2 Data Channels

Considerable efforts have been made for over the last decade to improve the spatial resolution of multispectral images beyond the intrinsic resolution of the original sensor. This has largely been done through spectral unmixing (e.g., [7]), fuzzy classifications with Hopfield neural networks (e.g., [8]), super-resolution variable-pixel linear reconstruction (e.g., [9]), down-scaling cokriging for super-resolution image mapping (e.g., [10]), hidden Markov tree model (e.g., [11]), or complex wavelet-domain image resolution enhancement algorithm (e.g., [12]). Efforts have also been made to fuse images at different resolutions, e.g., taking advantage of a panchromatic image to sharpen multiple spectral images at coarser resolutions (e.g., [13]–[18] or [19], among many others). This has prompted, in turn, attempts to evaluate the performance of these methods (e.g., [20] and [21]). In many cases, multiple low-resolution images (typically acquired in different spectral bands) are "sharpened" using a single (typically panchromatic) image at a higher spatial resolution. Similar interests have prompted parallel attempts in the thermal domain (e.g., [22]) as well as in the microwave spectral range (e.g., [23]). The situation with the MISR instrument is rather different because of the following: 1) all data channels are, in fact, acquired at the same spatial resolution by the sensor, although some are averaged

on-board before transmission to the ground segment; 2) our goal is not to sharpen existing channels beyond the intrinsic resolution of the MISR instrument but only to regenerate the measurements that were originally made; and 3) multiple channels at HR are available for the reconstruction of each reduced resolution channel. Improving the spatial resolution further remains possible, through fusion methods such as those mentioned previously or generalized approaches such as [24] or cokriging [25] for instance, but this lies outside our current scope.

Our "sharpening" step, i.e., the regeneration of data at the original spatial resolution (275 m) of the sensor in the 24 nonred spectral channels of the off-nadir cameras, capitalizes on the existence of three relevant channels at the native spatial resolution in the Terrain-projected L1B2 product: the red spectral band for the same camera $\rho_{\mathrm{red}}^{C}$, the same spectral band of the nadir pointing camera $\rho_{b}^{\mathrm{Nadir}}$, and the red spectral band of the nadir pointing camera $\rho_{\mathrm{red}}^{\mathrm{Nadir}}$.

The algorithm first synthesizes a spatial pattern of 16 HR values $R_b^C$, for each pixel of the 24 reduced resolution channels, using the three channels that are already available at the full resolution in L1B2

$$R_b^C = \rho_b^{\mathrm{Nadir}} \times \left[\rho_{\mathrm{red}}^{C} / \rho_{\mathrm{red}}^{\mathrm{Nadir}}\right] \tag{1}$$

where $b$ stands for the nonred spectral band and $C$ refers to the off-nadir camera. The assumption here is that the spatial patterns observable in the three data channels available at the full (native) spatial resolution are directly related to the unknown spatial pattern in the nonred and nonnadir channel. A simpler approach might consist in duplicating the pattern at nadir in the same spectral band, but that would ignore the angular variations that must affect the spectral values (e.g., the varying influence of shadows in the various cameras). Another method might be to duplicate the pattern observable for the same camera in the red spectral band, but that would incorrectly represent the natural spectral variations at any given angle (for instance, a vegetated HR pixel is expected to exhibit a lower reflectance in the red but a higher reflectance in near-infrared band than a bare ground pixel at any given angle). The linear scheme in (1) combines both approaches and attempts to minimize errors in each.

These 16 HR values are then adjusted in amplitude so that their spatial average $\langle R \rangle$ matches the observation $\rho_b^C$ reported for the corresponding reduced resolution (1.1 km) pixel in the GM data

$$r_b^C = R_b^C \times \left[\rho_b^C / \langle R \rangle\right] \tag{2}$$

where the 16 $r_b^C$ are the estimated pixel values at the full spatial resolution in that nonred $(b)$ spectral band and off-nadir $(C)$ camera. In mountainous areas, some of the HR pixels may be obscured from view by the topography at off-nadir angles: these are flagged, and $\rho_{\mathrm{red}}^{C}$ is set to zero in the process of generating the standard L1B2 product. These pixels will thus also have a null value in the other spectral bands.

### *B. Taking Atmospheric Effects Into Account*

The primary mission of the MISR instrument is to study the Earth atmosphere and, in particular, to characterize atmospheric aerosols and clouds. Significant efforts have thus been invested to address these issues in great detail (e.g., [26] and [27]). For the purpose of this paper, the cloud mask available from the standard processing has been used. It will be possible to improve on this in the future, as a higher spatial resolution may be beneficial to the detection and masking of small clouds, but that topic is outside the scope of this paper.

Standard level 2 aerosol products are typically generated at the 17.6-km spatial resolution, and standard level 2 surface products are available at the 1.1-km spatial resolution but only when the surface is actually observable from space (i.e., in the absence of clouds) and only wherever and whenever the characterization of atmospheric aerosols has been successful. When the latter does not get activated (due to cloud cover), fails to converge, or yields products that are not considered sufficiently reliable (as in the presence of complex topography), the entire 17.6 $\times$ 17.6 km region is skipped, and no standard level 2 surface product is generated.

Our treatment of aerosol effects exploits a software module developed and provided by the MISR Team at JPL. This code is available as part of the MISR toolkit and has also been used, e.g., by [28]. It was inspired by earlier work of [29] and [30], which describe the original ideas and provide information on the performance of the approach. The basic idea is to establish the correlation between the top of atmosphere (L1B2) and the surface (L2) bidirectional reflectances at the coarse spatial resolution of the standard products and to use those coefficients to convert the full spatial resolution TOA reflectances generated previously into full spatial resolution surface reflectances. This regression algorithm is applied independently to each camera and spectral band.

1) First, within each 17.6-km region (corresponding to the MISR L2 regional grid), the linear regression between the Terrain-projected top-of-atmosphere BRF (at 1100 m or averaged to that spatial resolution if the data are available at the 275-m resolution) and the land surface BRF (at 1100 m) is computed. This generates a grid of linear regression coefficients (intercepts $a_i$ and slopes $b_i$, with $i$ varying over the regions) at the 17.6-km spatial resolution.
2) The second step consists in smoothing this array of 17.6-km linear regression coefficients spatially over the entire MISR block, using a boxcar filter with a width of 3 pixels. This is justified by the fact that atmospheric properties tend to vary smoothly (compared to the surface) due to turbulence. This step also limits or prevents discontinuities (quilting) within the land surface products.
3) The smoothed linear regression coefficients are then interpolated to the resolution of the terrain data ($\alpha_j$ and $\beta_j$, with $j$ varying over the full spatial resolution pixels), using cubic convolution.
4) The interpolated linear regression coefficients are then applied to the Terrain-projected top-of-atmosphere

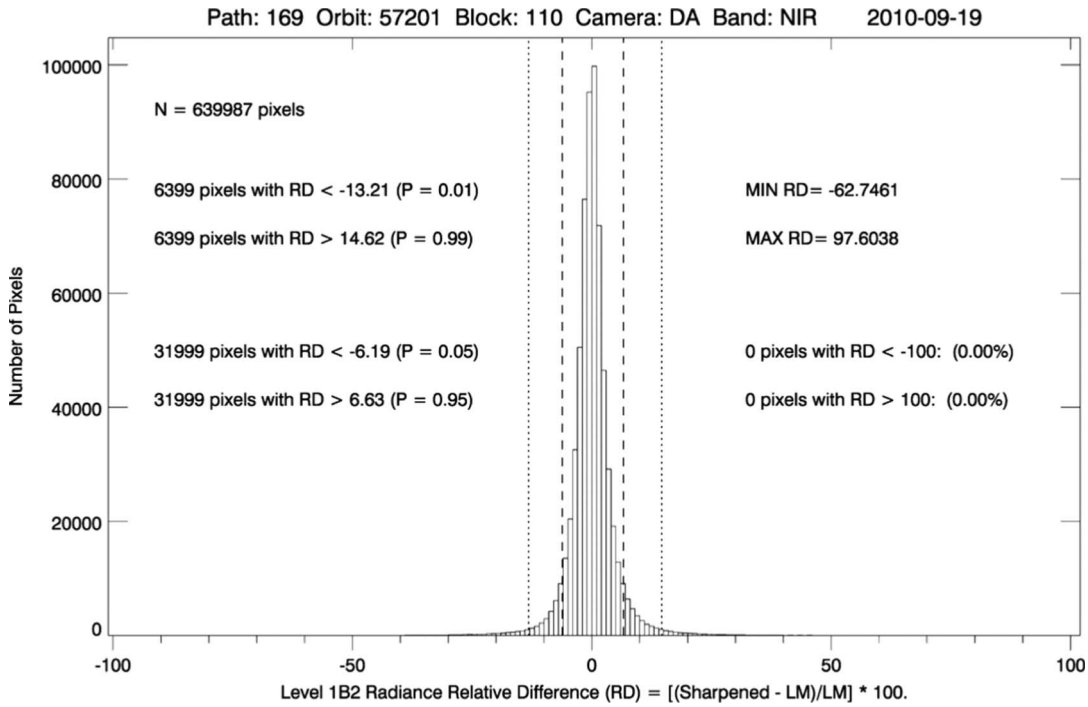


Fig. 2. Typical example of the RD between the sharpened GM and the LM data, in this case for Path 169, Orbit 57201, Block 110, Camera DA, in near infrared. Some 90% of the GM sharpened pixels differ by less than 6% from the corresponding LM values; other statistics are reported in the graph, which refers to a total of 639 967 pixels. Even better results are obtained in the other spectral bands (blue, green, and red) under clear sky conditions; larger RDs occur in the presence of scattered clouds (see text for details). The number of pixels with RD values smaller or larger than the 1st, 5th, 95th, and 99th percentiles (P) are also indicated.

reflectances to produce smoothed land surface reflectances at the 275-m resolution

$$\rho_{SFC}(j) = \alpha_j + \beta_j \times \rho_{TOA}(j). \quad (3)$$

5) Finally, if a pixel is identified as cloudy in the original L2 land surface reflectance product, this information is saved before this processing starts, and the corresponding full-resolution pixels are replaced by a fill value at the end of the procedure.

### C. Characterizing Surface Anisotropy

The Rahman–Pinty–Verstraete (RPV) model [31] is inverted against these full-resolution BRF values in each of the four spectral bands [32] to derive a quantitative description of the anisotropy of the observed surface in terms of the three parameters of that model: $\rho_0$, the amplitude or level of the BRF field; $k$, the Minnaert parameter [33] that indicates whether the surface bidirectional reflectance exhibits bowl-shaped or bell-shaped form; and $\Theta$, the asymmetry factor that indicates whether the observed target is scattering predominantly in the forward or backward direction. The RPV model has been found marginally better than the MRPV model currently used in the standard processing [34].

### D. Computing Broadband Albedos

Bihemispherical reflectance factors (albedos), assuming isotropic solar illumination, are calculated by integrating the RPV model over incoming and outgoing angles. These values are further adjusted to generate broadband (spectrally integrated) estimates in the visible and near-infrared spectral bands, using Liang's narrow to broadband conversion formulas [35].

### E. Applying the JRC-TIP

Finally, these broadband albedos are used as inputs by the Joint Research Centre Two-stream Inversion Package (JRC-TIP) software (described in [36]–[40]), which inverts a two-stream radiation transfer model by optimizing the values of its parameters through an assimilation procedure. This package generates internally consistent estimates of all radiation fluxes involved, including those scattered at the top of canopy and background level, transmitted through vegetation layers and absorbed in the canopy and background layers. The model parameters that achieve this optimization are the effective LAI and scattering properties of the vegetation layers (single scattering albedo), as well as the background albedo. The uncertainties associated with each estimate and the value of the cost function (a measure of the "goodness of fit") are also reported.

## V. Evaluation and Interpretation of the Results

### A. Assessment of the Sharpening Algorithm

To estimate the accuracy of the sharpening algorithm (step 1), we have compared the high spatial resolution reflectances derived at the "top of the atmosphere" from the L1B2 GM data with those generated by the LM acquisitions for each of the 36 data channels and for each of the 33 scenes available around the CSIR Skukuza research station. Fig. 2 shows one

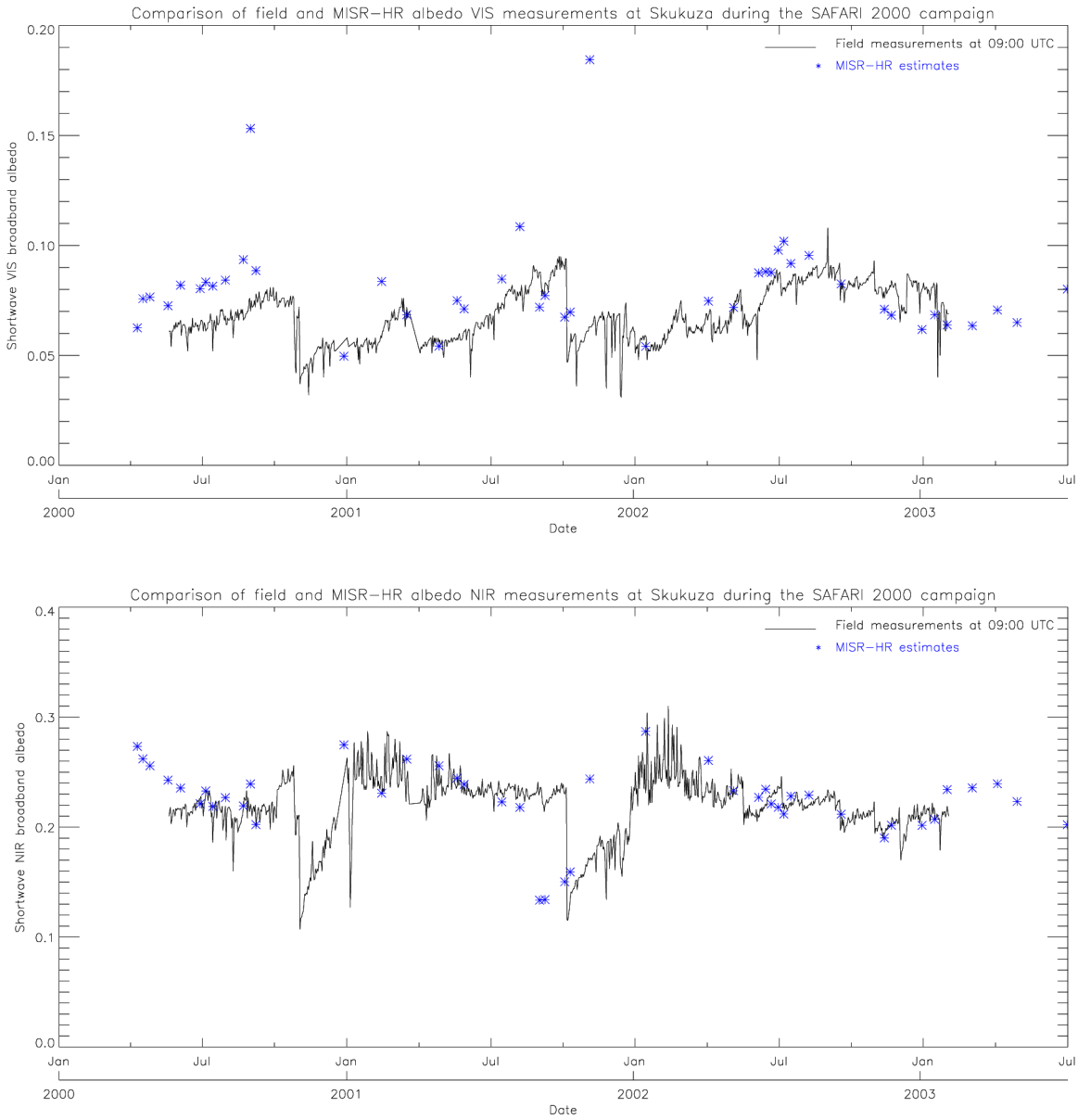


Fig. 3. Comparison between the albedo measurements in the visible and near-infrared spectral bands, acquired from the Skukuza flux tower and derived by the MISR-HR package, during the SAFARI-2000 campaign. Two retrievals (on August 31, 2000, and November 6, 2001) are considered outliers and, in fact, occur on days when significant cloudiness or smoke contaminates the remote sensing observations. The two sharp drops in field albedo (on November 2, 2000, and October 8, 2001) correspond to fire events. The agreement is reasonable, given the number of factors differentiating the measurements; see text for details.

of the 1200 histograms of relative differences (RDs) between the sharpened GM and the LM data, in this case from the DA camera in the near-infrared spectral band (a worst case angular and spectral scenario), for a clear sky scene (Path 169, Orbit 57201, Block 110 acquired on 19 September 2010). It can be seen that the RD between the two products is within 6% or so for 90% of the pixels in the block. When the scene is cloudy, these statistics degrade because parallax, due to the height of the cloud above the ground, causes the off-nadir camera to observe a different target than the nadir pointing camera (e.g., the ground versus the edge of a cloud). Since cloudy pixels are masked out anyway in subsequent processing, these discrepancies do not have any impact on the quality of the downstream surface products.

### *B. Assessment of the High Spatial Resolution Surface Products*

The main outcome of the subsequent processing thus consists in the generation of a suite of biogeophysical products describing the state and properties of land surfaces at the native spatial resolution of the MISR sensor (275 m), including a description of the anisotropy of the reflected radiation field (the three parameters of the RPV model) and the albedo of the environment at the top of the canopy, in the four spectral bands of the instrument and in the two broad visible and near-infrared bands, as well as the leaf single scattering albedo, the effective LAI, the FAPAR, the albedo of the soil background, and the reflected, transmitted, and absorbed fluxes of radiation in the canopy, in these broad spectral bands, each

accompanied by uncertainty estimates and the value of the cost function, a measure of the goodness of fit between the model and the observations. The *algorithms* used to generate these products have been published before, and their performance has been evaluated in other contexts (e.g., [34], [39], and [40]).

A preliminary indication of the accuracy of the MISR-HR *products* can be gathered by inspecting Fig. 3, which compares field measurements of surface albedo (continuous line) acquired with Kipp and Zonen CM14 albedometers mounted at the end of a 2.5-m-long horizontal boom, pointing northward, at the top of the 20-m-high tower at the Skukuza research site in the Kruger National Park, South Africa [6], [41], with the MISR-HR retrieval of the bihemispherical reflectance, in the visible (top panel) and near-infrared (bottom panel) spectral bands. It will be seen that two outliers are present, on August 31, 2000, and November 6, 2001, respectively. Close inspection of the corresponding MISR scenes showed that the measurements for the pixel closest to the Skukuza flux tower were very likely contaminated by clouds and smoke in these two cases. The two major drops in albedo correspond to fire events (see, e.g., [42]).

While the general agreement between these two estimates of albedo appears satisfactory, especially in the second half of the period, a number of factors must be kept in mind while interpreting such a graph, including the following.

1) The size of the areas actually observed by the two sensors is quite different. According to [6], the downward pointing pyranometer sampled a circular area of about 170 m of diameter (2.27 ha), while the nominal area of a MISR-HR pixel on the ground is 7.56 ha.
2) The centers of these two areas do not coincide either, as the MISR-HR values correspond to the pixel values closest to the tower coordinates (which may be on the order of 100 m away from the tower).
3) The spectral bands of the two instruments are different, with "PAR" values from the field albedometers derived from differences between total shortwave (300–2800 nm) and near-infrared (700–2800 nm) values, while MISR values in the visible and near-infrared broadbands are estimated on the basis of weighted averages of three (four) spectral narrowband measurements, as explained previously.
4) Skukuza's original NIR albedometer was found to be degrading early in the campaign and was replaced with a new one on August 27, 2000.
5) Field instruments were only occasionally cleaned so that measurements could be affected by dust accumulation, especially in the dry season.
6) Raw measurements from the field albedometers were converted into physical values using factory calibration information.
7) No adjustments were applied to the field measurements to correct for the contribution of the flux tower itself or its shadow to the measurements or for possibly not perfectly level sensor, largely due to lack of knowledge or characterization of these effects.
8) While the position of a given pixel on a specific orbit is known with an accuracy of about 100 m or so, the pixels closest from the flux tower on orbits belonging to the different paths may themselves be centered on slightly different locations.

Direct comparisons between field and space measurements are fraught with difficulties and require very careful detailed measurement protocols, especially in environments that include substantial spatial heterogeneity [43]. It must be pointed out, however, that considerable efforts have been made to evaluate the performance of the JRC-TIP in a variety of environments (e.g., [44]).

### C. Using the HR Products

This suite of MISR-derived biogeophysical products offers key advantages over both the standard products already available from the same instrument and those generated by other global sensors: they are physically based, internally consistent, and available at a spatial resolution (275 m) that is of greater interest and relevance to ecologists than the traditional products at 1.1 km, without compromising the temporal frequency of acquisition associated with instruments operating at higher spatial resolution. Some of these products are exhibited here as examples of what is systematically being generated.

Fig. 4 shows maps of the Minnaert $k$ parameter of the RPV model, in the red spectral band, for an area of 30.525 by 30.525 km (101-by-101 full-resolution pixels) around CSIR's Skukuza flux tower site on two different dates. Reddish tones indicate a bowl-shaped anisotropy, bluish tones indicate a bell-shaped anisotropy, and white areas are close to Lambertian. The appearance of bell-shaped reflectance field in December 2006 (left panel) is a rare event in this environment and is thought to reflect a temporary high degree of heterogeneity in the vegetation pattern (see [45] and [46]). The April 2009 pattern (right panel) is typical of the area during the dry season. Less drastic changes but noticeable spatial patterns are observed in every scene and reflect the diversity of the landscape, particularly the type and density of trees in this savanna environment.

Fig. 5 shows maps of the land surface broadband albedo, in the visible (left) and near infrared (right), for the same area around the Skukuza research site, derived from observations acquired on April 25, 2009 (Path 169, Orbit 49745, Block 110). The degraded areas associated with the human settlements just outside the Kruger National Park, in the north-western corner of the map, are characterized by a higher albedo than the unmanaged land inside the park.

Having processed Blocks 110 and 111 of all orbits of Paths 168 and 169 for the first ten years of operation of MISR, it is possible to extract time series of any one of these products. The temporal evolution of the mean retrieved FAPAR and the associated standard deviation for the full-resolution pixel located on the Skukuza flux site is shown in Fig. 6 as an example. The seasonal variations are noticeable, and the year-to-year fluctuations are consistent with the precipitation amounts accumulated during the corresponding wet seasons (November 1 to April 30 of the following year).

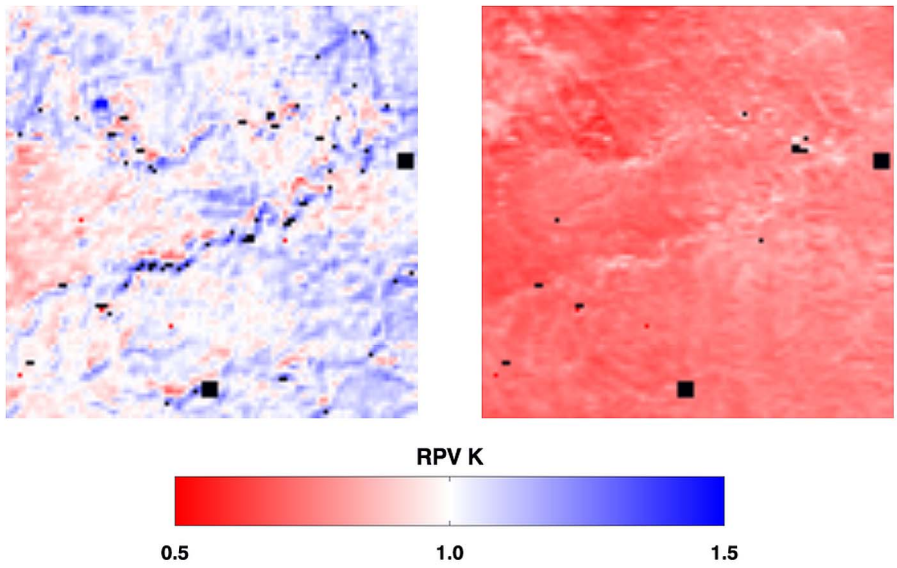


Fig. 4. Maps of the Minnaert $k$ parameter of the RPV model in the red spectral band for an area of 30.525 by 30.525 km (101-by-101 full-resolution pixels) around CSIR's Skukuza flux tower site, derived from observations acquired on December 13, 2006 (left; Path 169, Orbit 37163, Block 110), and April 25, 2009 (right; Path 169, Orbit 49745, Block 110). Reddish tones indicate a bowl-shaped anisotropy, bluish tones indicate a bell-shaped anisotropy, and white areas are close to Lambertian.

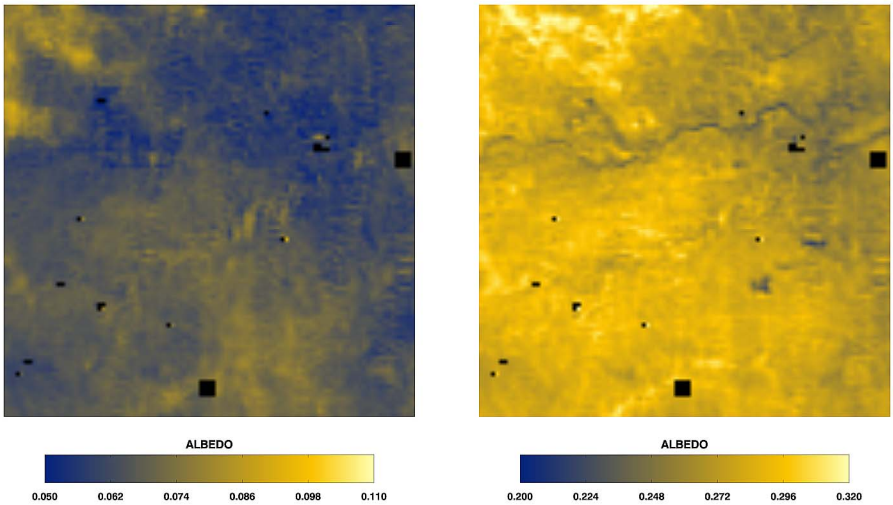


Fig. 5. Land surface albedo in the visible (left panel) and near infrared (right panel) for the whole environment (soil and vegetation) for an area of 30.525 by 30.525 km (101-by-101 full-resolution pixels) around CSIR's Skukuza flux tower site, derived from observations acquired on April 25, 2009 (Path 169, Orbit 49745, Block 110).

## VI. Conclusion

The MISR instrument has been in essentially continuous operation for over a decade. The standard land surface products are generated at a spatial resolution of 1.1 km because 24 of its 36 raw measurements for each pixel are transmitted to the ground segment at that resolution. However, the sensors on the focal plane work at the native spatial resolution of 275 m, and in fact, 12 of the data channels are actually downloaded at this native resolution. This paper shows that it is possible to regenerate all 36 data channels (4 spectral bands in each of 9 cameras) of the MISR instrument at the full spatial resolution. The performance of our sharpening algorithm has been evaluated by comparing these results with the data acquired in LM, i.e., when all channels are also temporarily acquired at the full resolution, and it has been shown that the RD between the sharpened GM product (available everywhere and all the time) and the LM product (obtainable only upon request and for limited areas) is on the order of a few percents in cloud-free areas. This technique opens the way to a host of downstream applications that can take advantage of this higher spatial resolution and exploit 36 spectrodirectional data channels to derive products at the 275-m resolution for any location observed by MISR and any time since February 2000.

A couple of blocks (110 and 111) of MISR data covering northeastern South Africa and southwestern Mozambique were acquired for Paths 168 and 169 and for all orbits during the first ten years of operation of the MISR instrument. An entirely new processing system was implemented to generate a suite of products at high spatial resolution (275 m), including 36 spectral and directional reflectance fields, both at the top and at

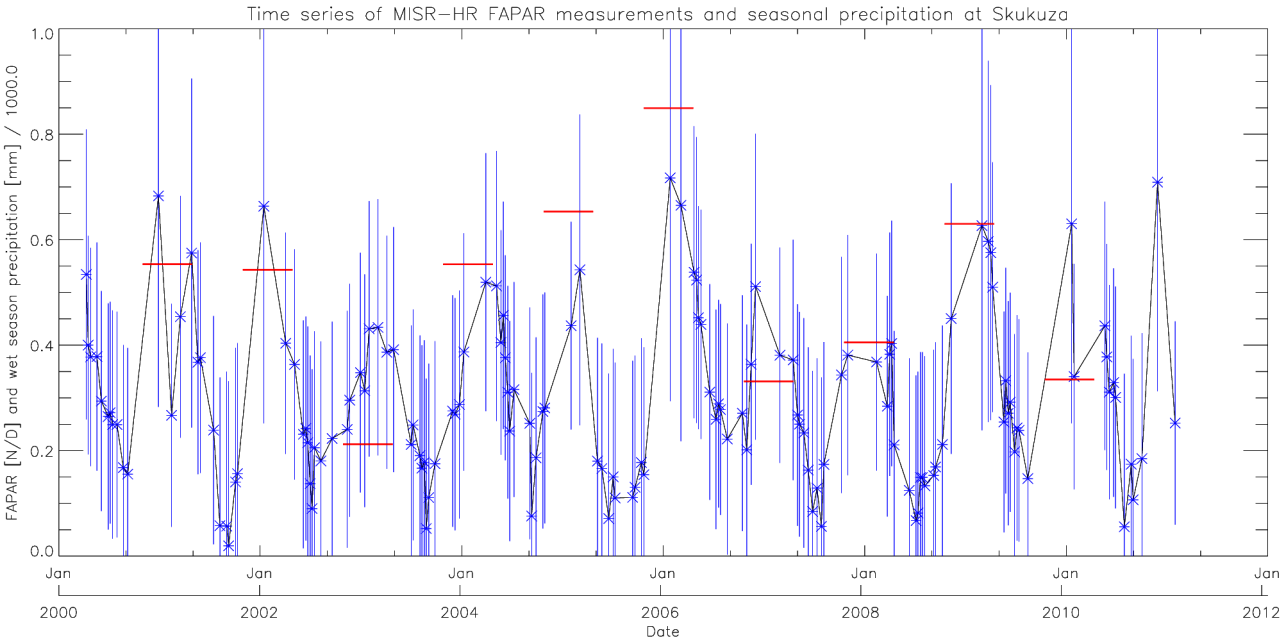


Fig. 6. Time series of mean posterior FAPAR value and associated standard deviation for the full-resolution pixel located at the Skukuza flux tower. The values reported here for that location were derived from MISR observations in Paths 168 and 169, during the first decade of operation of that instrument. The horizontal lines represent the accumulated precipitation, in millimeters divided by 1000 to fit the vertical scale, during the corresponding wet seasons (November 1 to April 30 of the following year).

the bottom of the atmosphere, a characterization of the surface anisotropy (through inversion of the RPV model in each of the four spectral bands), broadband albedos (bihemispherical reflectances) in the visible and near-infrared spectral bands, and all standard products of the JRC-TIP algorithm, including the effective LAI of the canopy, the fraction of absorbed photosynthetically active radiation (FAPAR), the optical properties of the leaves, and the albedo of the background under the canopy, as well as error bars for all of these variables and an estimate of the goodness of fit of the model to the data.

Some of these products have been exhibited as examples; they provide a unique and rather exhaustive characterization of the radiation environment over the target area. Derived HR products such as FAPAR and LAI are of great interest to ecologists because they provide more detail than the traditional land surface products at 1.1 km and yet remain available at a temporal frequency relevant to the study of the evolution of living systems. For instance, at that resolution, it is possible to document subtle ecological differences between the top and bottom of the catena, which have different dominant tree species, or critical environmental factors such as burned scars, the evolution of desertification, or the expansion of urban areas near the border of the Kruger National Park.

This new processing system is being installed at the recently created South African National Space Agency (SANSA), which intends to generate these products systematically for the African continent for the entire period of operation of the MISR instrument.

## ACKNOWLEDGMENT

The authors would like to thank M. Bull of JPL for providing a version of the software module used in this paper to implement atmospheric corrections to the L1B2 data as part of the MISR Toolkit, as well as V. Jovanovic and M. Garay, also from JPL, for the useful discussions on the sharpening algorithm. D. McDonald of JPL is responsible for the MISR LM acquisitions, and he was instrumental in providing systematic coverage of the Skukuza site since December 2009. W. Lück of SANSA provided pointers to the literature on super-resolution and image fusion. All MISR data were obtained from the Atmospheric Science Data Center, NASA Langley Research Center. The authors would also like to thank their respective institutions for the on-going support for this interdisciplinary and international collaboration, and the various anonymous reviewers for their help in improving this manuscript. M. M. Verstraete gratefully acknowledges the continuing support of the Joint Research Centre (JRC) and the hospitality of the Natural Resources and the Environment, Council for Scientific and Industrial Research, during his sabbatical stay in South Africa. L. A. Hunt is most thankful for the travel support provided by the Institute for the Protection and Security of the Citizens and the Institute for Environment and Sustainability, JRC, European Commission, over the last few years.

## REFERENCES

[1] D. J. Diner, M. M. Verstraete, and J. V. Martonchik, "Foreword to special section on MISR," *IEEE Trans. Geosci. Remote Sens.*, vol. 40, no. 7, pp. 1447–1448, Jul. 2002.

[2] D. J. Diner, L. Di Girolamo, and A. Nolin, "Preface to the MISR special issue," *Remote Sens. Environ.*, vol. 107, no. 1/2, p. 1, Mar. 2007.

[3] D. J. Diner, J. C. Beckert, T. H. Reilly, C. J. Bruegge, J. E. Conel, R. A. Kahn, J. V. Martonchik, T. P. Ackerman, R. Davies, S. A. W. Gerstl, H. R. Gordon, J.-P. Muller, R. B. Myneni, P. J. Sellers, B. Pinty, and M. M. Verstraete, "Multi-angle Imaging SpectroRadiometer (MISR) instrument description and experiment overview," *IEEE Trans. Geosci. Remote Sens.*, vol. 36, no. 4, pp. 1072–1087, Jul. 1998.

[4] R. J. Scholes, N. Gureja, M. Giannecchinni, D. Dovie, B. Wilson, N. Davidson, K. Piggott, C. McLoughlin, K. van der Velde, A. Freeman, S. Bradley, R. Smart, and S. Ndala, "The environment and vegetation of

the flux measurement site near Skukuza, Kruger National Park," *Koedoe*, vol. 44, no. 1, pp. 73–83, 2001.

[5] R. J. Swap, H. J. Annegarn, J. T. Suttles, M. D. King, S. Platnick, J. L. Privette, and R. J. Scholes, "Africa burning: A thematic analysis of the Southern African regional science initiative (SAFARI 2000)," *J. Geophys. Res.*, vol. 108, no. D13, p. 8465, Jul. 2003.

[6] J. L. Privette, M. Mukelabai, N. Hanan, and Z. Hao, "SAFARI 2000 surface albedo and radiation fluxes at Mongu and Skukuza, 2000–2002," NASA, Washington, DC, Tech. Rep., 2005, data set available from the Oak Ridge National Laboratory (ORNL Distributed Active Archive Center (DAAC).

[7] A. Boucher, P. C. Kyriakidis, and C. C. Cronkite-Ratcliff, "Geostatistical solutions for super-resolution land cover mapping," *IEEE Trans. Geosci. Remote Sens.*, vol. 46, no. 1, pp. 272–283, Jan. 2008.

[8] A. J. Tatem, H. G. Lewis, P. M. Atkinson, and M. S. Nixon, "Super-resolution target identification from remotely sensed images using a Hopfield neural network," *IEEE Trans. Geosci. Remote Sens.*, vol. 39, no. 4, pp. 781–796, Apr. 2001.

[9] M. T. Merino and N. Nunez, "Super-resolution of remotely sensed images with variable-pixel linear reconstruction," *IEEE Trans. Geosci. Remote Sens.*, vol. 45, no. 5, pp. 1446–1457, May 2007.

[10] P. M. Atkinson, E. Pardo-Igúzquiza, and M. Chica-Olmo, "Downscaling cokriging for super-resolution mapping of continua in remotely sensed images," *IEEE Trans. Geosci. Remote Sens.*, vol. 46, no. 2, pp. 573–580, Jan. 2008.

[11] F. Li, X. Jia, D. Fraser, and A. Lambert, "Super resolution for remote sensing images based on a universal hidden Markov tree model," *IEEE Trans. Geosci. Remote Sens.*, vol. 48, no. 3, pp. 1270–1278, Mar. 2010.

[12] T. Celik and T. Tjahjadi, "Image resolution enhancement using dual-tree complex wavelet transform," *IEEE Geosci. Remote Sens. Lett.*, vol. 7, no. 3, pp. 554–557, Jul. 2010.

[13] J. C. Price, "Combining multispectral data of differing spatial resolution," *IEEE Trans. Geosci. Remote Sens.*, vol. 37, no. 3, pp. 1199–1203, May 1999.

[14] A. K. Shackelford and C. H. Davis, "A hierarchical fuzzy classification approach for high-resolution multispectral data over urban areas," *IEEE Trans. Geosci. Remote Sens.*, vol. 41, no. 9, pp. 1920–1932, Sep. 2003.

[15] A. K. Shackelford and C. H. Davis, "A combined fuzzy pixel-based and object-based approach for classification of high-resolution multispectral data over urban areas," *IEEE Trans. Geosci. Remote Sens.*, vol. 41, no. 10, pp. 2354–2363, Oct. 2003.

[16] A. S. Kumar, A. S. Kiran Kumar, and R. R. Navalgund, "Selection of IRS-P6 LISS-4 MO mode band for producing band-sharpened multispectral imagery," *IEEE Geosci. Remote Sens. Lett.*, vol. 3, no. 1, pp. 32–35, Jan. 2006.

[17] C. Thomas, T. Ranchin, L. Wald, and J. Chanussot, "Synthesis of multispectral images to high spatial resolution: A critical review of fusion methods based on remote sensing physics," *IEEE Trans. Geosci. Remote Sens.*, vol. 46, no. 5, pp. 1301–1312, May 2008.

[18] M. Joshi and A. Jalobeanu, "MAP estimation for multiresolution fusion in remotely sensed images using an IGMRF prior model," *IEEE Trans. Geosci. Remote Sens.*, vol. 48, no. 3, pp. 1245–1255, Mar. 2010.

[19] A. G. Mahyari and M. Yazdi, "Panchromatic and multispectral image fusion based on maximization of both spectral and spatial similarities," *IEEE Trans. Geosci. Remote Sens.*, vol. 49, no. 6, pp. 1976–1985, Jun. 2011.

[20] L. Alparone, S. Baronti, A. Garzelli, and F. Nencini, "A global quality measurement of pan-sharpened multispectral imagery," *IEEE Geosci. Remote Sens. Lett.*, vol. 1, no. 4, pp. 313–317, Oct. 2004.

[21] Q. Du, N. H. Younan, R. King, and V. P. Shah, "On the performance evaluation of pan-sharpening techniques," *IEEE Geosci. Remote Sens. Lett.*, vol. 4, no. 4, pp. 518–522, Oct. 2007.

[22] W. Zhan, Y. Chen, J. Zhou, J. Li, and W. Liu, "Sharpening thermal imageries: A generalized theoretical framework from an assimilation perspective," *IEEE Trans. Geosci. Remote Sens.*, vol. 49, no. 2, pp. 773–789, Feb. 2011.

[23] B.-G. Lim, J.-C. Woo, and Y.-S. Kim, "Noniterative super-resolution technique combining SVA with modified geometric mean filter," *IEEE Geosci. Remote Sens. Lett.*, vol. 7, no. 4, pp. 713–717, Oct. 2010.

[24] X. Zhu, J. Chen, F. Gao, X. Chen, and J. G. Masek, "An enhanced spatial and temporal adaptive reflectance fusion model for complex heterogeneous regions," *Remote Sens. Environ.*, vol. 114, no. 11, pp. 2610–2623, Nov. 2010.

[25] E. Pardo-Igúzquiza, M. Chica-Olmo, and P. M. Atkinson, "Downscaling cokriging for image sharpening," *Remote Sens. Environ.*, vol. 102, no. 1/2, pp. 86–98, May 2006.

[26] J. V. Martonchik, D. J. Diner, K. A. Crean, and M. A. Bull, "Regional aerosol retrieval results from MISR," *IEEE Trans. Geosci. Remote Sens.*, vol. 40, no. 7, pp. 1520–1531, Jul. 2002.

[27] R. A. Kahn, M. J. Garay, D. L. Nelson, K. K. Yau, M. A. Bull, B. J. Gaitley, J. V. Martonchik, and R. C. Levy, "Satellite-derived aerosol optical depth over dark water from MISR and MODIS: Comparisons with AERONET and implications for climatological studies," *J. Geophys. Res.*, vol. 112, p. D18 205, Sep. 2007.

[28] M. Chopping, A. Nolin, G. G. Moisen, J. V. Martonchik, and M. Bull, "Forest canopy height from the Multiangle Imaging SpectroRadiometer (MISR) assessed with high resolution discrete return lidar," *Remote Sens. Environ.*, vol. 113, no. 10, pp. 2172–2185, Oct. 2009.

[29] J. D. Armston, S. R. Phinn, P. F. Scarth, and T. J. Danaher, "Analysis of Multiangle Imaging SpectroRadiometer (MISR) measurements in the Queensland Southern Brigalow belt," in *Proc. 12th Australasian Remote Sens. Photogramm. Conf.*, Fremantle, Australia, Oct. 18–22, 2004, pp. 1–14.

[30] J. D. Armston, P. F. Scarth, S. R. Phinna, and T. J. Danaher, "Analysis of multi-date MISR measurements for forest and woodland communities, Queensland, Australia," *Remote Sens. Environ.*, vol. 107, no. 1/2, pp. 287–298, Mar. 2007.

[31] H. Rahman, B. Pinty, and M. M. Verstraete, "Coupled surface-atmosphere reflectance (CSAR) model 2. Semiempirical surface model usable with NOAA Advanced Very High Resolution Radiometer data," *J. Geophys. Res.*, vol. 98, no. D11, pp. 20 791–20 801, 1993.

[32] T. Lavergne, T. Kaminski, B. Pinty, M. Taberner, N. Gobron, M. M. Verstraete, M. Vobeck, J.-L. Widlowski, and R. Giering, "Application to MISR land products of an RPV model inversion package using the Adjoint and Hessian codes," *Remote Sens. Environ.*, vol. 107, no. 1/2, pp. 362–375, Mar. 2007.

[33] M. Minnaert, "The reciprocity principle in Lunar photometry," *Astrophys. J.*, vol. 93, pp. 403–410, May 1941.

[34] O. Engelsen, B. Pinty, M. M. Verstraete, and J. V. Martonchik, Parametric bidirectional reflectance factor models: Evaluation, improvements and applications, Brussels, Belgium1996.

[35] S. Liang, C. J. Shuey, A. L. Russ, H. Fang, M. Chen, C. L. Walthall, C. S. T. Daughtry, and R. Hunt, Jr., "Narrowband to broadband conversions of land surface albedo—II Validation," *Remote Sens. Environ.*, vol. 84, no. 1, pp. 25–41, Jan. 2003.

[36] B. Pinty, T. Lavergne, M. Vobeck, T. Kaminski, O. Aussedat, R. Giering, N. Gobron, M. Taberner, M. M. Verstraete, and J.-L. Widlowski, "Retrieving surface parameters for climate models from Moderate Resolution Imaging Spectroradiometer (MODIS)–Multiangle Imaging SpectroRadiometer (MISR) albedo products," *J. Geophys. Res.*, vol. 112, p. D10 116, May 2007.

[37] B. Pinty, T. Lavergne, T. Kaminski, O. Aussedat, R. Giering, N. Gobron, M. Taberner, M. M. Verstraete, M. Vobeck, and J.-L. Widlowski, "Partitioning the solar radiant fluxes in forest canopies in the presence of snow," *J. Geophys. Res.*, vol. 113, p. D04 104, Feb. 2008.

[38] M. Clerici, M. Vobeck, B. Pinty, T. Kaminski, M. Taberner, T. Lavergne, and I. Andredakis, "Consolidating the two-stream inversion package (JRC-TIP) to retrieve land surface parameters from albedo products," *IEEE J. Sel. Topics Appl. Earth Observ. Remote Sens.*, vol. 3, no. 3, pp. 286–295, Sep. 2010.

[39] B. Pinty, I. Andredakis, M. Clerici, T. Kaminski, M. Taberner, M. M. Verstraete, N. Gobron, S. Plummer, and J.-L. Widlowski, "Exploiting the MODIS albedos with the two-stream inversion package (JRC–TIP): 1. Effective leaf area index, vegetation, and soil properties," *J. Geophys. Res.*, vol. 116, p. D09 105, May 2011.

[40] B. Pinty, M. Clerici, I. Andredakis, T. Kaminski, M. Taberner, M. M. Verstraete, N. Gobron, S. Plummer, and J.-L. Widlowski, "Exploiting the MODIS albedos with the two-stream inversion package (JRC-TIP): 2. Fractions of transmitted and absorbed fluxes in the vegetation and soil layers," *J. Geophys. Res.*, vol. 116, p. D09 106, May 2011.

[41] M. O. Román, C. B. Schaaf, P. Lewis, F. Gao, G. P. Anderson, J. L. Privette, A. H. Strahler, C. E. Woodcock, and M. Barnsley, "Assessing the coupling between surface albedo derived from MODIS and the fraction of diffuse skylight over spatially-characterized landscapes," *Remote Sens. Environ.*, vol. 114, no. 4, pp. 738–760, Apr. 2010.

[42] S. A. Archibald, A. Kirton, M. R. van der Merwe, R. J. Scholes, C. A. Williams, and N. Hanan, "Drivers of inter-annual variability in net ecosystem exchange in a semi-arid savanna ecosystem, South Africa," *Biogeosciences*, vol. 6, pp. 251–266, 2009.

[43] J.-L. Widlowski, "On the bias of instantaneous FAPAR estimates in open-canopy forests," *Agric. Forest Meteorol.*, vol. 150, no. 12, pp. 1501–1522, Dec. 2010.

[44] B. Pinty, M. Jung, T. Kaminski, T. Lavergne, M. Mund, S. Plummer, E. Thomas, and J.-L. Widlowski, "Evaluation of the JRC-TIP 0.01 ° products over a mid-latitude deciduous forest site," *Remote Sens. Environ.*, vol. 115, no. 12, pp. 3567–3581, Dec. 2011.
[45] B. Pinty, J.-L. Widlowski, N. Gobron, M. M. Verstraete, and D. J. Diner, "Uniqueness of multi-angular measurements. Part 1: An indicator of subpixel surface heterogeneity from MISR," *IEEE Trans. Geosci. Remote Sens.*, vol. 40, no. 7, pp. 1560–1573, Jul. 2002.
[46] N. Gobron, B. Pinty, M. M. Verstraete, J.-L. Widlowski, and D. J. Diner, "Uniqueness of multi-angular measurements. Part 2: Joint retrieval of vegetation structure and photosynthetic activity from MISR," *IEEE Trans. Geosci. Remote Sens.*, vol. 40, no. 7, pp. 1574–1592, Jul. 2002.

**Michel M. Verstraete** (SM'03) received the "License en Physique" from the Université Catholique de Louvain, Louvain-la-Neuve, Belgium, in 1974, the "Licence Spéciale en Géophysique" from the Université Libre de Bruxelles, Brussels, Belgium, 1976, and the M.Sc. degree in meteorology and the D.Sc. degree in atmospheric sciences from the Massachusetts Institute of Technology, Cambridge, in 1978 and 1985, respectively.

He was with the World Meteorological Organization, Geneva, Switzerland, and Nairobi, Kenya, in 1979–1981; with the National Center for Atmospheric Research, Boulder, CO, in 1982–1989; and with the University of Michigan, Ann Arbor, MI, in 1989–1990. He is currently with the Institute for Environment and Sustainability, Joint Research Centre, European Commission, Ispra, Italy. His initial work on topics such as the modeling of atmosphere–biosphere interactions and desertification led him to his current interest in the quantitative exploitation of satellite remote sensing data for the characterization of terrestrial surface properties.

Dr. Verstraete is a member of various scientific advisory committees including the Global Climate Observing System and has had a long association with Space Agencies, especially the European Space Agency (MERIS Scientific Advisory Group), EUMETSAT, and NASA/JPL (MISR Science Team).

**Linda A. Hunt** received the B.A. degree in economics, the M.S. degree in computer science, and the M.S. degree in atmospheric science from the College of William and Mary, Williamsburg, VA, in 1974, 1980, and 1999, respectively.

She has been with the NASA Langley Research Center, Hampton, VA, since 1980 and is currently a Senior Computer Scientist with the Science Systems and Applications, Inc., Hampton, where she is involved with research on the energy budget and chemistry of the thermosphere and mesosphere, primarily with data from the Sounding of the Atmosphere Broadband Emission and Radiometry instrument. Her work with the Multi-angle Imaging SpectroRadiometer (MISR) instrument team and data while at the NASA Langley Atmospheric Science Data Center led to her collaboration with the EC Joint Research Centre and the South African National Space Agency in developing advanced MISR processing for land surface properties.

**Robert J. Scholes** received the Ph.D. degree from the University of the Witwatersrand, Johannesburg, South Africa, in 1988.

He is cureently a Systems Ecologist with the Council for Scientific and Industrial Research, Pretoria, South Africa. His research interests involve the global carbon cycle, particularly the carbon exchange in African savannas. He has been involved in the design of Earth Observation systems for many years, including contributions to the Global Terrestrial Observing System and the Global Earth Observation System of Systems. He is currently the Chair of the GEO Biodiversity Observation Network.

**Marco Clerici** received the B.S. degree (with honors) in electronic engineering, specializing in microelectronics and instrumentation, from the Politecnico di Milano, Milan, Italy, in 1993.

He was with EUMETSAT from 2000 to 2004, providing software development support for the MSG/SEVIRI vicarious calibration and for the development of radiative transfer models. He is currently with the Institute for Environment and Sustainability, Joint Research Centre, European Commission, Ispra, Italy. His work focuses on the implementation of operational algorithms and systems for the land and vegetation characterization from remote sensing, applied to the global and continental scale, with a focus on applications for the African continent.

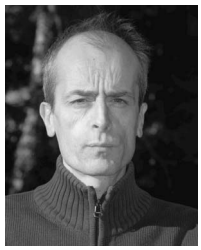

**Bernard Pinty** received the Maîtrise de Chimie and DEA, thèse de troisième cycle en Physique de l'Atmosphère, and thèse d'Etat from the Université Blaise Pascal, Clermont-Ferrand, France, in 1977, 1980, and 1988, respectively.

He visited the National Center for Atmospheric Research, Boulder, CO, from 1988 to 1989, served as the Deputy Director of the Laboratoire d'Etudes et de Recherches en Télédétection Spatiale (LERTS), Toulouse, France, from 1990 to 1992, and was appointed as Full Professor of physics with the Université Blaise Pascal, Clermont-Ferrand, France, in 1993. He is currently with the Institute for Environment and Sustainability, Ispra, Italy, and was seconded in 2011 to the Earth Observation Directorate of the European Space Agency (ESA) at ESRIN, Frascati, Italy. He is the author or coauthor of over 130 refereed publications. His main interests currently include research on the theory of radiation transfer in plant canopies and, more generally, the development of tools to quantitatively interpret satellite remote sensing data in the optical spectral domain via inverse methods. He is a member of the MERIS Scientific Advisory Group of ESA and a member of the MISR Science Team of NASA/JPL.

Dr. Pinty was the recipient of the Zel'dovich medal from COSPAR in 1990. In 2002, he was awarded both the "Group Achievement Award" by NASA and the "ENVISAT Medal" by ESA.

**David L. Nelson** received the M.S. degree in geology from the California Institute of Technology, Pasadena.

He is currently a Senior Data Analyst and Applications Programmer with Raytheon Intelligence and Information Systems, Pasadena, where he has worked with the Multi-angle Imaging SpectroRadiometer (MISR) team at the NASA Jet Propulsion Laboratory, Pasadena, for 12 years. Among other contributions, he is the principal author of the MINX tool for retrieving plume heights, winds, and physical properties from MISR data. He has also been a codeveloper of the MISR Research Aerosol Retrieval Algorithm and a contributor to software development on several of MISR's production data products.